The influence of BN additives on the phase composition, microstructure and mechanical properties of 316L steel consolidated by spark plasma sintering

IOP Conf. Series: Materials Science and Engineering **426** (2018) 012020 doi:10.1088/1757-899X/426/1/012020

The influence of BN additives on the phase composition, microstructure and mechanical properties of 316L steel consolidated by spark plasma sintering

P Jenei[1], Cs Balázsi[2], Á Horváth[2], K Balázsi[2] and J Gubicza[1]

[1] Eötvös Loránd University, Department of Materials Physics, Budapest, Hungary
[2] Hungarian Academy of Sciences, Centre for Energy Research, Budapest, Hungary

E-mail: jenei@metal.elte.hu

Abstract. Blends of commercial 316L steel and boron nitride (BN) were consolidated using Spark Plasma Sintering (SPS). The components were mixed by high energy milling (using attritor) before sintering. The aim was to study the effect of BN on the microstructure and the mechanical properties. Two composites containing 0.5 and 2 wt.% BN were produced beside a pure 316L specimen. It was found that bimodal grain size distribution formed during the production. A bcc α'-phase formed during milling beside the main fcc γ-phase. The addition of BN resulted in a slightly higher dislocation density and a smaller grain size in the fine grained parts of the samples. At the same time, the elastic modulus and the strength determined by bending test were reduced, most probably due to the weak bonding between the 316L and the BN grains, and the lower fraction of α'-phase.

1. Introduction

Ceramic dispersion strengthened steels are promising structural materials in new generation nuclear reactors and future fusion power plants [1–4]. Since the nanoscale (~10 nm) ceramic particles are thermally stable, therefore it can obstruct the movement of dislocations and prevent the grain growth even at high temperatures, thereby hindering both recovery and recrystallization. Hence this steels have excellent strength at high temperatures (even under neutron radiation [5]), however the low ductility and fracture toughness limit their industrial applications [6]. Beside the oxide particles, other filler materials can also be used for the improvement of the functional properties of steels [4,6,7]. For instance, boron nitride (BN) additive can increase the absorption of neutrons in the steel composites [8].

The steel composites strengthened by particles are usually produced by powder metallurgy methods [1,2,9,10]. The components of the matrix and the disperse phase are blended by mechanical milling, which is usually followed by a high-temperature consolidation process. During milling the initially small grain sized particles are fragmented and a part of them can dissolve into the matrix [9]. The microstructure of the matrix and the disperse phase depends strongly on the circumstances of the production of the material, therefore they determine the mechanical properties. The components are often consolidated by Spark Plasma Sintering (SPS) [1]. During SPS pulses of high current density are used to facilitate consolidation, thus the sintering time and temperature decrease, therefore much smaller grain size can be achieved compared to conventional sintering methods [11].

In the present study, the effect of BN additive on the microstructure and the mechanical behavior of 316L steel was investigated. The samples were produced by powder metallurgy using high energy milling and SPS. The microstructure was investigated by electron backscattered diffraction (EBSD) and X-ray line profile analysis (XLPA). The mechanical behavior was characterized by microhardness measurement and three point bending test. The effect of the phase composition, the porosity, the grain size and the dislocation density on the mechanical properties will be discussed.

2. Materials and experimental procedures

2.1. Sample preparation

The samples were processed from a commercial 316L austenitic stainless steel powder (manufacturer: Höganäs) with the composition of Fe – 16.8 % Cr – 12 % Ni – 2.5 % Mo – 1.5 % Mn – 0.6 % Si – 0.0025 % C (wt.%). The disperse phase in the composites was an ultrafine-grained (UFG) boron nitride (BN) powder obtained from a hexagonal boron nitride (hBN) (manufacturer: H.C. Starck). First, the starting 316L powder was intensively milled in a DMQ-07 attritor (manufacturer: Union Process) at 2800 rpm for 10 hours in propanol. In this machine, a stainless steel setup with delta disk agitators were used. The diameters of the stainless steel grinding balls were 1 mm. After sieving in a 100 micron mesh, the powder was milled in a dry environment for 1 hour at 600 rpm in 01-HD/HDDM type attritor (manufacturer: Union Process).

The UFG BN powder was prepared by mechanical milling. First, the commercial hBN powder was milled intensively in a high efficient attritor mill (01-HD/HDDM type attritor) equipped with zirconia agitator delta discs and zirconia grinding media (1 mm in diameter) in the presence of ethanol at 4000 rpm for 10 h. After wet milling, a dry milling process was applied at 4000 rpm for 5 h. Finally, a UFG BN powder with an average grain size of ~200 nm was achieved, as can be seen in figure 1a.

After this milling process, 0.5 and 2 wt.% BN were added to the 316L powder and this powder blend was further milled in the 01-HD/HDDM type attritor equipped with stainless steel tank, delta disk agitators and grinding media with 1 mm in diameter. The high energy milling was performed at 4000 rpm for 3 hours in ethanol in order to achieve an efficient dispersion of the boron nitride in the commercial 316L powder. Finally, the milled powders were sieved in a 100 micron mesh. A reference 316L powder was also processed without the addition of BN powder. However, this powder was subjected to the same milling process as the blends of 316L and BN powders. The milling process resulted in flat particles with the thickness of about 200 nm (see figure 1b).

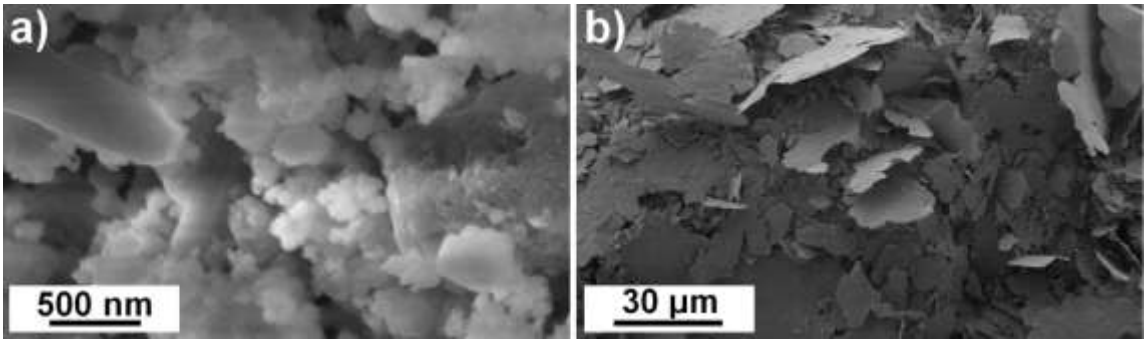

Figure 1. SEM images taken on the milled a) BN and b) 316L+2BN powder.

The powders were sintered by SPS in vacuum at 900 ± 10°C for 5 minutes under a pressure of 50 MPa. SPS-processing was carried out by an SPS-7.40MK-VII machine (manufacturer: SPS Syntex Inc.) installed in Istanbul Technical University using a current of 20,000 A. Disks with 50 mm in diameter and 5 mm in thickness were obtained after the consolidation process. In the following, the samples containing 0, 0.5 and 2 wt.% BN are referred to as 316L, 316L+0.5BN and 316L+2BN, respectively.

2.2. Microstructure investigations

The microstructure of the samples was studied by X-ray diffraction, Scanning Electron Microscopy (SEM) and EBSD. The mass density of the sintered samples was measured in water using Archimedes' principle. The phase composition of the samples was investigated by a Philips Xpert ($\lambda = 0.15418$ nm) X-ray powder diffractometer. The microstructure of the main γ-phase was studied by XLPA. The X-ray line profiles were measured by a high-resolution diffractometer using $CoK\alpha_1$ ($\lambda = 0.1789$ nm) radiation. For this measurement, the samples were electropolished in an A8 electrolytic solution at room temperature at a fixed voltage of 10 V for 30 s. Two-dimensional imaging plates detected the Debye-Scherrer diffraction rings. The line profiles were evaluated by the Convolutional Multiple Whole Profile (CMWP) method. The details of the CMWP procedure can be found in Refs. [12,13]. In this method, the experimental pattern is fitted by the convolution of the instrumental pattern and the theoretical size and strain line profiles. The instrumental pattern was measured on a LaB_6 line profile standard material. The theoretical profile functions used in this fitting procedure are calculated on the basis of a model of the microstructure, where the crystallites have spherical shape and log-normal size distribution, and the lattice strains are assumed to be caused by dislocations. As an example, the CMWP fitting for the sample 316L+2BN in a logarithmic intensity scale is shown in figure 2. The open circles and the solid line represent the measured data and the fitted curve, respectively.

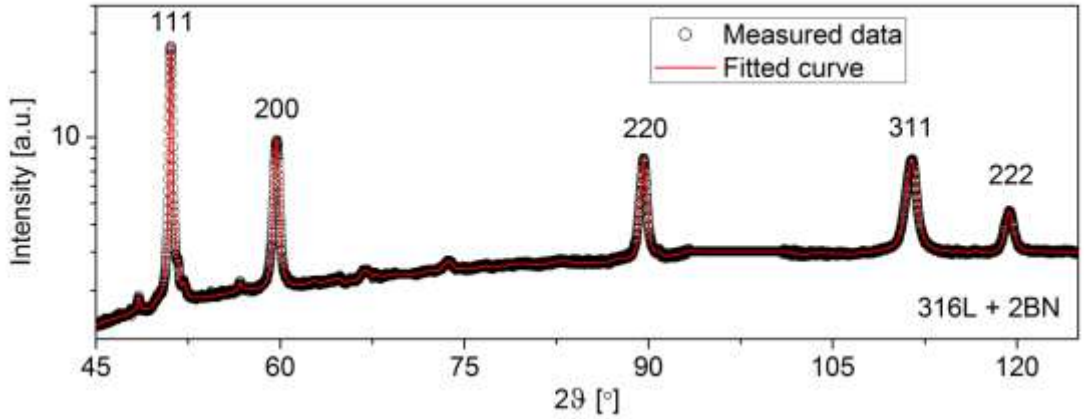

Figure 2. CMWP fitting of the X-ray diffraction pattern taken on the sample 316L+2BN. The open circles and the solid line represent the measured data and the fitted curve, respectively.

The EBSD analysis was performed using an FEI Quanta 3D dual beam SEM equipped with an EDAX type EBSD system. The surface of the sample was mechanically polished (steps: P1000, P2500, P4000, 1μm ALOX, Mastermet2 suspension (about 30 nm SiC, manufactured by Stuers)). The grain size was determined from the EBSD scans using OIM software from TexSEM Laboratories. The morphology of the powder particles was studied by SEM (Zeiss-SMT LEO 1540 XB and Jeol JSM-25-SIII).

2.3. Mechanical tests

The Vickers hardness of the samples was measured on electropolished surfaces using a Zwick Roell ZHμ Vickers indenter with an applied load of 300 g and a dwell time of 10 s. For the bending test, rectangular bars with the dimensions of $4 \times 4 \times 50$ mm^3 were cut from the sintered specimens using a water-jet cutting process. The three-point bending strength was determined by an Instron 1112 tensile/loading machine equipped with a data acquisition system.

3. Results and discussion

3.1. Phase composition and porosity

In all specimens, the main phase was an fcc Fe-based alloy (denoted as γ-phase) but in addition bcc Fe-based alloy (denoted as α'-phase), Fe_3O_4 and $Cr_{23}C_6$ phases were also identified. As an example, figure

3a shows a part of the X-ray diffraction pattern obtained for the 316L+0.5BN sample. It should be noted that BN was not detected, most probably due to the fragmentation of the BN particles during high-energy milling as well as the very small amount of this phase.

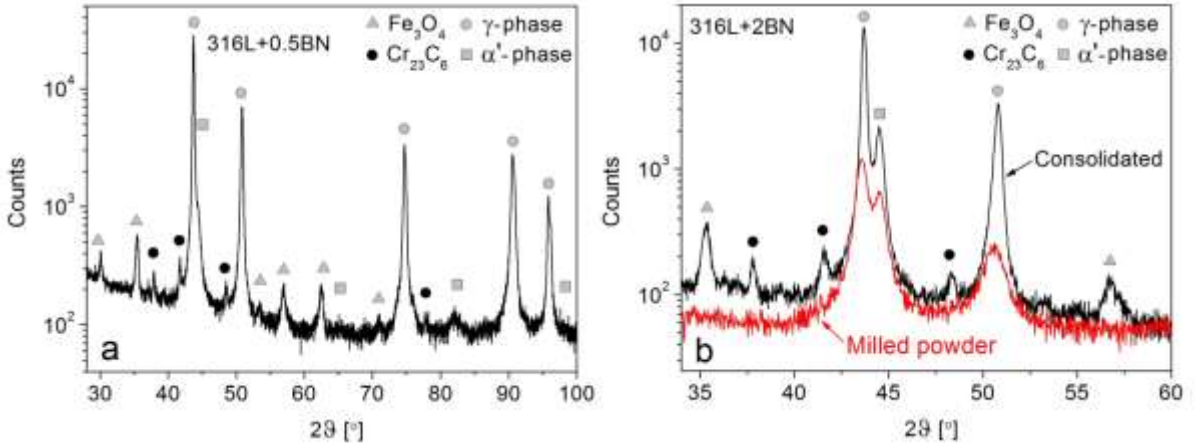

Figure 3. (a) X-ray diffractogram for the sample 316L+0.5BN. (b) A part of the X-ray diffractogram obtained for the sample 316L+2BN before and after consolidation.

In order to reveal the influence of the additives on the phase composition, the fractions of the integrated intensities for the different phases in the X-ray diffractograms were determined and listed Table 1 for all samples. In all milled powders (irrespectively of the additives), the fractions of γ-phase and α'-phase were 0.73 and 0.27, respectively (see Table 1). It is noted that the intensity fractions of the phases are not equivalent with their volume fractions. The addition of BN to 316L steel resulted in a slight increase of the fraction of γ-phase while the amount of the secondary α'-phase decreased. The α'-phase was formed during milling due to deformation induced martensitic transformation. However, at the high temperature of SPS the γ-phase is more stable, therefore there is an α' to γ reverse phase transformation as it can be seen in figure 3b. In the milled powder, beside the γ-phase only a secondary α'-phase was detected. At the same time, after consolidation the fraction of α'-phase decreased and Fe_3O_4 and $Cr_{23}C_6$ peaks appeared on the diffractogram. It seems that the addition of BN promotes the α' to γ transformation. A reasonable explanation of this effect may be that the BN grains serve as nuclei in the phase transformation during sintering.

Table 1. The fractions of the integrated intensities for the different phases and the porosity of the consolidated samples.

Sample	γ-phase	α'-phase	Fe_3O_4	$Cr_{23}C_6$	Porosity [%]
Milled powders	0.73 ± 0.02	0.27 ± 0.02	-	-	-
316L	0.81 ± 0.05	0.14 ± 0.02	0.04 ± 0.01	0.01 ± 0.01	5.4 ± 0.3
316L+0.5BN	0.93 ± 0.03	0.03 ± 0.01	0.03 ± 0.01	0.01 ± 0.01	4.4 ± 0.3
316L+2BN	0.88 ± 0.05	0.07 ± 0.02	0.03 ± 0.01	0.01± 0.01	5.3 ± 0.3

The porosity was calculated from the difference between the measured and calculated densities. In the case of the composite specimens, the calculated density was obtained as an average of the theoretical densities of 316L iron (7.99 g/cm^3) and BN (3.45 g/cm^3) weighted by their mass fractions. Table 1 shows that BN have no significant effect on the porosity of the consolidated samples.

3.2. Microstructure

3.2.1 EBSD investigation. The SEM investigations on the polished surfaces revealed that all samples exhibit bimodal grain structures as can be seen in Fig 4b, e and h. In the matrix, the light and dark regions correspond to coarse-grained (CG) and fine-grained (FG) regions, respectively. Coarse particles were

also observed in the initial 316L powder. The EBSD images in figure 4 show that both regions are fragmented into grains. The grain sizes were evaluated from these images and listed in Table 2. It can be seen that the grain size is much higher in the CG regions for all samples. The BN additive resulted in a lower grain size as the BN grains hinder the recovery and recrystallization of the microstructure during sintering.

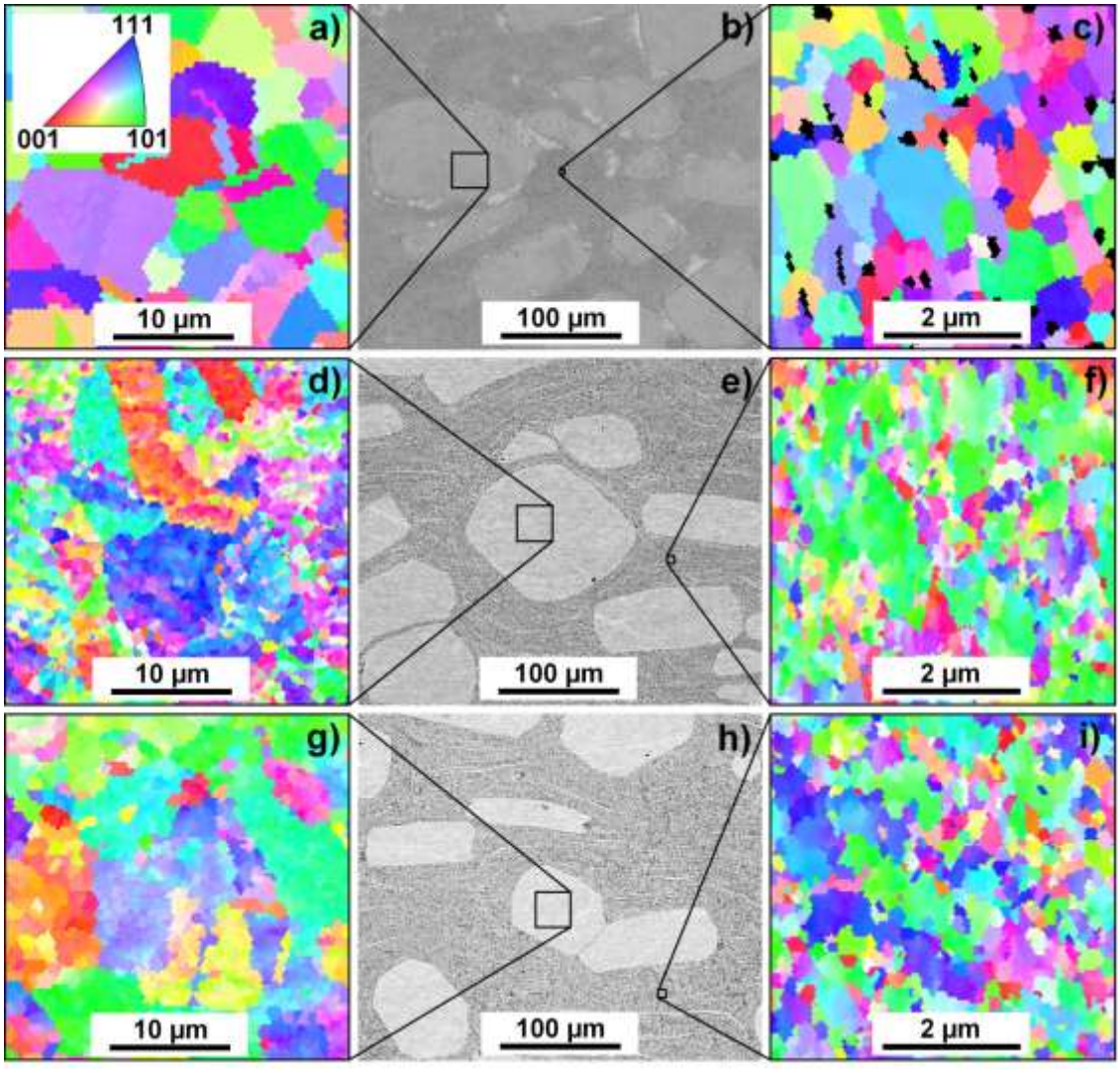

Figure 4. EBSD and SEM images showing the morphology of the grains in the CG and FG regions for the sample (a-c) 316L, (d-f) 316L+0.5BN and (g-i) 316L+2BN. The color code of the standard stereographic triangle inset in (a) illustrates the grain orientations in the gamma-phase. The black regions in Fig. 4c are occupied by α'-phase.

Table 2. The grain size values in the fine-grained (d_{FG}) and the coarse-grained (d_{CG}) regions determined by EBSD. The dislocation density (ρ_{UFG}) in the ultrafine grained (UFG) regions of γ-phase as obtained by XLPA, and the intensity fraction of the UFG parts of the microstructures (f_{UFG}). The total dislocation density (ρ_{total}) in the γ-phase was determined as the product of ρ_{FG} and f_{FG}.

Sample	d_{FG} [µm]	d_{CG} [µm]	ρ_{UFG} [10^{14} m^{-2}]	f_{UFG}	ρ_{total} [10^{14} m^{-2}]
316L	0.44	3.66	6.3 ± 0.7	0.68 ± 0.05	4.3 ± 0.8
316L+0.5BN	0.23	0.93	5.0 ± 0.6	0.65 ± 0.05	3.3 ± 0.7
316L+2BN	0.28	1.71	7.5 ± 0.9	1	7.5 ± 0.9

3.2.2. X-ray line profile analysis. The dislocation density was determined for the γ-phase and listed in Table 2. It should be noted that for the pure 316L and 316L+0.5BN specimens, the intensity distribution along the Debye–Scherrer (DS) rings was inhomogeneous and numerous sharp intensity spots were visible as it can be seen in figure 5b. These sharp peaks were as narrow as the instrumental broadening ($\Delta(2\theta)=0.03°$); therefore they were not evaluated for the microstructure. These sharp intensity spots are related to regions in which the crystallite size is larger and the dislocation density is lower than the detection limits of XLPA for the present experimental setup (800 nm and 10^{13} m^{-2}, respectively).

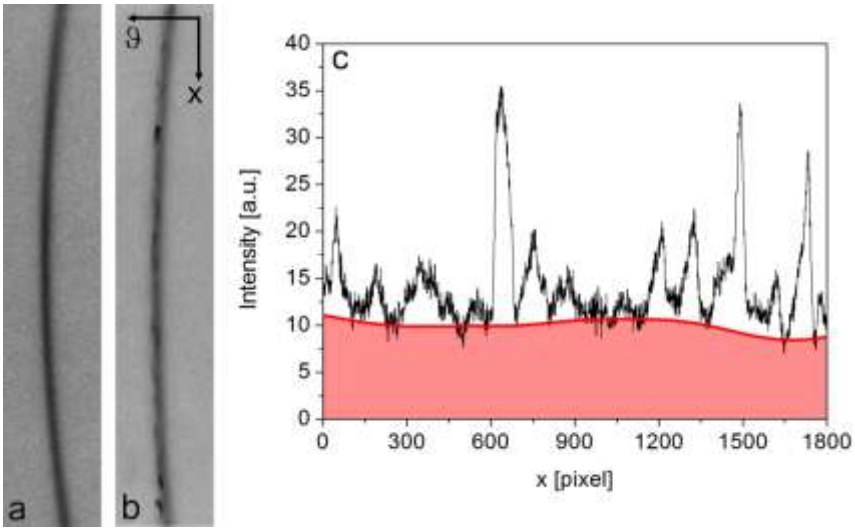

Figure 5. Debye–Scherrer diffraction rings of reflection 200 for the samples (a) 316L+2BN and (b) 316L+0.5BN. (c) Intensity distribution in direction *x* in figure (b) after subtracting the background. The red zone corresponds to the homogeneous and broad ring segments in (b) scattered from the UFG region.

Due to the spotty diffraction rings for the pure 316L and the 316L+0.5%BN samples, only the broader and more homogeneous parts between the large intensity spots were evaluated by XLPA. As a consequence, the results obtained for these two samples characterize only the ultrafine grained (UFG) part of the samples. It should be noted that the UFG region may be located in either the CG or the FG area. The total dislocation densities in the whole materials can be calculated by considering the UFG fractions in the samples. This quantity can be estimated as the fraction of the intensities of the homogeneous parts in the entire DS ring. The intensity was summed in direction 2ϑ (see figure 5b), and these intensity values were plotted as a function of the coordinate *x*, as shown in figure 5c for reflection 200 of the sample 316L+0.5BN. Thereafter, a spline was fitted to the parts of the intensity distribution which are free of sharp intensity peaks (see figure 5c). The area under this spline corresponds to the intensity scattered from the UFG parts of the sample. The fractions of the UFG parts for the pure 316L and the 316L+0.5BN samples are listed in Table 2. For the 316L+2BN sample, the DS rings were homogeneous (see figure 5a) therefore for this specimen the microstructural parameters determined by XLPA characterize the whole specimens (i.e., the fraction of the UFG parts is 1). Then, the total dislocation density was calculated as the product of the dislocation density in the UFG regions and their intensity fraction. Table 2 shows that the addition of 0.5 wt.% BN did not yield a considerable change in the total dislocation density. At the same time, 2 wt.% BN resulted in a higher dislocation density than in the addition-free 316L steel due to the pinning effect of BN particles.

It should be noted that there is an apparent discrepancy. It can be seen in Table 2, that the grain size measured by EBSD is higher for the sample 316L+2BN than in the specimen 316+0.5BN, while the DS rings are homogeneous in the sample 316L+2BN and spotty in the specimen 316L+0.5BN. This can be explained by the fact that the grains in EBSD investigation were defined as the regions bounded by high angle grain boundaries with misorientation angles higher than 15°. In the case of XLPA, the crystallites

are the domains which scatter X-rays coherently. As the coherency of X-rays breaks even if they are scattered from volumes having quite small misorientations (1–2°), the crystallites correspond rather to the subgrains in the microstructures [14]. Therefore, most probably the subgrain structure is finer in the 316L+2BN sample, which can not be evaluated by EBSD.

3.3. Mechanical properties

Table 3 shows the average hardness measured for the FG and CG regions for all samples. In addition, the Young's modulus and the three-point bending strength are also listed in Table 3. Generally, the hardness is higher in the FG parts of the samples due to the lower grain size. It can be seen that the addition of 0.5% BN has no significant effect on the mechanical properties of 316L steel. At the same time, 2% BN resulted in a reduction of the Young's modulus and the bending strength. This can be explained by the lower fraction of α'-phase and the weak bonding between the BN and the 316L grains, which can promote crack formation and propagation during the bending test.

Table 3. The mechanical properties of 316L samples sintered with and without BN additive.

Sample	Young's modulus [GPa]	Three-point bending strength [MPa]	HV [GPa] Coarse-grained	HV [GPa] Fine-grained
316L	183 ± 5	1324 ± 28	2.55 ± 0.13	3.80 ± 0.10
316L+0.5BN	174 ± 2	1265 ± 58	2.65 ± 0.14	3.41 ± 0.15
316L+2BN	166 ± 2	1066 ± 45	2.36 ± 0.12	3.30 ± 0.15

It is worth to note that despite the very different microstructures in the studied samples, the hardness values only slightly vary with increasing the BN content. There are four main microstructure features which can influence considerably the mechanical properties: (1) the phase composition (the α'-phase content in our case), (2) the dislocation density in the main γ-phase, (3) the grain size and (4) the porosity. Table 4 shows the relative contributions of the different microstructural features to the hardness.

Table 4. The relative hardening effects of the microstructural features in the samples. The more '+' icons indicate a stronger hardening effect as compared to the other samples.

Hardening effects	316L	316L+0.5BN	316L+2BN
α'-phase fraction	+++	+	++
Relative density	+	++	+
Dislocation density	++	+	+++
Grain size	+	+++	++

It can be seen that for the sample 316L+0.5BN, the porosity, the total dislocation density in the γ-phase and the grain size were only slightly lower than in the pure 316L sample. Therefore, the smaller hardness in the FG region can be attributed to the higher γ to α'-phase ratio. It is well known that the γ-phase is softer than the α'-phase in 316L steel. For the sample 316L+2BN, the porosity is the same as for the pure 316L steel but the dislocation density is higher and the grain size is lower due to the addition of BN. Despite the much higher dislocation density, the hardness of the specimen 316L+2BN is slightly lower than for the sample 316L which indicates that the softening effect of the larger γ-phase fraction overwhelms the hardening effect of the higher dislocation density and the lower grain size. Comparing the two composites, for the sample 316L+2BN the hardening effects of the dislocation density and the α'-phase content were higher, while the contributions of the grain size and the porosity to the hardness were lower than for the specimen 316L+0.5BN, which can explain their similar hardness values.

4. Summary

The effect of BN addition on the microstructure and the mechanical properties of commercial 316L stainless steel was studied. Samples containing 0, 0.5 and 2 wt.% BN were produced using high energy milling and SPS method. The following results were obtained:

1) A high fraction (27-28 %) of α'-phase formed beside the major γ-phase phase during the milling process. During sintering at high temperature, the fraction of the α'-phase decreased due to a reverse martensitic phase transformation. It seems that the BN additive promotes this transformation since the fraction of α'-phase is considerably lower in the composites. Fe_3O_4 and $Cr_{23}C_6$ phases were also formed during the consolidation process.

2) All samples show inhomogeneous grain structure. Large particles can be seen in the fine grained matrix. The larger particles are fragmented into smaller grains. The addition of 0.5% BN decreased the grain size in both regions, but further BN addition did not result in a finer grain structure. The microhardness of the fine grained part was higher (irrespectively of the BN content) duo to the much lower grain size.

3) The addition of 0.5% BN did not result in a significant change in the dislocation density. The increase of the BN content from 0.5 to 2% yielded a higher dislocation density due to the hindering effect of BN particles on the annihilation of dislocations during sintering. The microhardness, the bending strength and the elastic modulus slightly decreased with increasing the BN content. This effect can be attributed mainly to the lower α'-phase fraction and the weak bonding between the 316L and the BN grains.

Acknowledgment
The authors are indebted to the National Research, Development, and Innovation Office Grant nos. K-109021, PD-121049 and MTA EK project „Nanostructural ODS steel development" for financial support. The authors thank to preparation of samples to V. Varga, SEM investigation to L. Illés, EBSD measurements to Á. Szabó and sintering to Prof. F. C. Sahin. JP acknowledges the financial support of the Hungarian Ministry of Human Capacities under Grant no. NTP-NFTÖ-16-0957.

References

[1] Balázsi C, Gillemot F, Horváth M, Wéber F, Balázsi K, Sahin FC, Onüralp Y and Horváth Á. 2011 *J. Mater. Sci.* **46**:4598
[2] Mukhopadhyay DK, Froes FH and Gelles DS 1998 *J. Nucl. Mater.* **258-263**:1209
[3] Renzetti R, Sandim HRZ, Bolmaro RE, Suzuki P and Möslang A 2012 *Mater. Sci. Eng. A* **534** 142
[4] Zhong Z, Hinoki H, Park YH and Kohyama A 2010 *Fusion Eng. Des.* **85** 992
[5] Monnet I, Dubuisson P, Serruys Y, Ruault MO, Kaı¨tasov O and Jouffrey B 2004 *J. Nucl. Mater.* **335** 311
[6] Mahathanabodee S, Palathai T, Raadnui S, Tongsri R and Sombatsompop N 2014 *Wear* **316** 37
[7] Patankar SN, Chandrasekaran M and Tan MJ. 2000 *J. Mater. Sci. Lett.* **19** 613
[8] Narayana Rao M. 2011 *Energy Procedia* **7** 199
[9] Alinger MJ, Odette GR and Hoelzer DT 2009 *Acta Mater.* **57** 392
[10] Rahmanifard R, Farhangi H and Javad A 2015 *J. Alloys Compd.* **622** 948
[11] Orrù R, Licheri R, Locci AM, Cincotti A and Cao G. 2009 *Mater. Sci. Eng. R Reports* **63** 127
[12] Ribárik G, Gubicza J and Ungár T 2004 *Mater. Sci. Eng. A* **387-389** 343
[13] Ungar T, Gubicza J, Ribárik G and Borbély A 2001 *J. Appl. Crystallogr.* **34** 298
[14] Ungár T, Tichy G, Gubicza J and Hellmig RJ 2012 *Powder. Diffr.* **20** 366